

Diamagnetism, Nernst signal, and finite size effects in superconductors above the transition temperature T_c

T. Schneider^{1,*} and S. Weyeneth¹

¹*Physik-Institut der Universität Zürich, Winterthurerstrasse 190, CH-8057 Zürich, Switzerland*

Various superconductors, including cuprate superconductors, exhibit peculiar features above the transition temperature T_c . In particular the observation of a large diamagnetism and Nernst signal N in a wide temperature window above T_c attracted considerable attention. Noting that this temperature window exceeds the fluctuation dominated regime drastically and that in these materials the spatial extent of homogeneity is limited, we explore the relevance of the zero dimensional (0D)-model, neglecting thermal fluctuations. It is shown that both, the full 0D-model as well as its Gaussian approximation, mimic the essential features of the isothermal magnetization curves $m_d(H)$ in Pb nanoparticles and various cuprates remarkably well. This analysis also provides estimates for the spatial extent of the homogeneous domains giving rise to a smeared transition in zero magnetic field. The resulting estimates for the amplitude of the in-plane correlation length exhibit a doping dependence reflecting the flow to the quantum phase transition in the underdoped limit. Furthermore it is shown that the isothermal Nernst signal of a superconducting $\text{Nb}_{0.15}\text{Si}_{0.85}$ film, treated as $N \propto -m_d$, is fully consistent with this scenario. Accordingly, the observed diamagnetism above T_c in Pb nanoparticles, in the cuprates $\text{La}_{1.91}\text{Sr}_{0.09}\text{CuO}_4$ and $\text{BiSr}_2\text{Ca}_2\text{CuO}_{8-\delta}$, as well as the Nernst signal in $\text{Nb}_{0.15}\text{Si}_{0.85}$ films, are all in excellent agreement with the scaling properties emerging from the 0D-model, giving a universal perspective on the interplay between diamagnetism, Nernst signal, correlation length, and the limited spatial extent of homogeneity. Our analysis also provides evidence that singlet Cooper pairs subjected to orbital pair breaking in a 0D system are the main source of the observed diamagnetism and Nernst signal in an extended temperature window above T_c .

PACS numbers: 74.25.Bt, 74.81.-g, 75.20.-g

I. INTRODUCTION

The detection of Cooper pairs above the superconducting transition temperature T_c has a long history, dating back to 1969.¹ It implies that the average of the order parameter squared, $\langle |\psi|^2 \rangle$, does not vanish above T_c , either due to thermal fluctuations or the limited effective spatial extent of the system. While the regime where thermal fluctuations dominate is reasonably well understood in terms of the scaling theory of critical phenomena subjected to finite size effects,²⁻⁹ novel features have been observed considerably outside the fluctuation dominated regime. Recently, Li *et al.*^{10,11} have compiled the results of an extended experimental study of the isothermal magnetization of several families of cuprate superconductors over a rather broad range of temperatures and magnetic fields. From these, they infer that above the transition temperature T_c , the isothermal diamagnetic contribution to the magnetization m_d decreases initially with increasing magnetic field H , applied parallel to the c -axis, consistent with $m_d = -\chi_d H$, where χ_d is the diamagnetic susceptibility. However, as H increases m_d tends to a minimum at H_m and in excess of this characteristic field the magnetization increases and appears to approach zero, as shown in Fig. 1 for $\text{La}_{1.91}\text{Sr}_{0.09}\text{CuO}_4$, showing data taken from Li *et al.*¹¹

Closely related behavior was reported earlier for oriented powder samples of underdoped $\text{Y}_{1-x}\text{Ca}_x\text{Ba}_2\text{Cu}_3\text{O}_y$,¹² for Pb nanoparticles with particle size larger than the correlation length,¹³ for

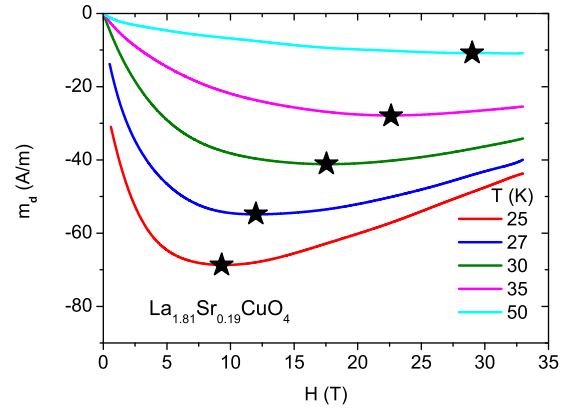


FIG. 1: (color online) The solid lines show isotherms m_d vs. H at various temperatures above $T_c \simeq 23$ K for $\text{La}_{1.91}\text{Sr}_{0.09}\text{CuO}_4$ taken from Li *et al.*¹¹. The symbol \star indicates the minimum in the curves for the presented isotherms.

MgB_2 ,¹⁴ and for polycrystalline $\text{SmBa}_2\text{Cu}_{3-y}\text{Al}_y\text{O}_{6+\delta}$.¹⁵ The magnetization was either inferred from torque magnetometry,^{10,11} or probed by SQUID magnetometry.^{12,13,15} However, the torque measurements reveal a temperature dependent paramagnetic background $m_p(T, H)$. The diamagnetic contribution to the magnetization is then derived from¹¹

$$m_d(T, H) = m_{\text{exp}}(T, H) - m_p(T, H), \quad (1)$$

where

$$m_p(T, H) \simeq (a + bT)H, \quad a \gg bT. \quad (2)$$

Although this subtraction leads to uncertainties in the high field limit, where the diamagnetic signal becomes small, it appears unlikely that the main feature, the occurrence of the minimum in $m_d(T, H)$ at fixed temperature $T > T_c$, is an artifact of this subtraction. Although the crossover from the initial linear ($m_d = -\chi_d H$) to nonlinear behavior is an expected feature of thermal fluctuations in homogeneous two (2D) and three (3D) dimensional superconductors, the occurrence of the minimum cannot be explained invoking these scenarios.²⁻⁷ On the other hand, there is considerable evidence that cuprate and amorphous conventional superconductors are homogeneous over a limited spatial domain only.^{8,16-22} In this case, the growth of the correlation lengths is limited by approaching the transition temperature T_c because it cannot exceed the respective extent of the homogeneous domains. Within a two dimensional superconductor, consisting of a stack of superconducting layers with insulating spacing sheets in between, the adoption of this scenario where the magnetization stems from homogeneous domains with limited extent only would result in an effective 0D-superconductor. As a consequence, the isothermal magnetization curves would exhibit a minimum, reminiscent to the observation in nanoparticles.¹³

Related behavior was also observed in the isothermal Nernst signal of superconducting and amorphous $\text{Nb}_{0.15}\text{Si}_{0.85}$ films above T_c .²³⁻²⁵ In this system, the Nernst signal due to normal quasiparticles is particularly low. This allows to probe the contribution associated with superconductivity without the subtraction of the background due to the normal quasiparticles.²³⁻²⁵ At low magnetic field, the Nernst signal $N = \nu H$ increases linearly with field, where ν is the Nernst coefficient. Upon increasing the magnetic field, N deviates from this linear field dependence, reaches a maximum at H_m and decreases afterwards. In analogy to the position of the minimum in the magnetization, the maximum shifts to higher fields with increasing temperature. This behavior confirms the evidence that the isothermal Nernst signal is proportional to the magnetization in terms of $N \propto -m_d$.^{26,28-30}

Here we review the properties of the isothermal magnetization curves of a 0D-superconductor, neglecting thermal fluctuations, and explore the consistency with experimental magnetization data of Pb nanoparticles,¹³ bulk $\text{La}_{1.91}\text{Sr}_{0.09}\text{CuO}_4$,¹¹ and $\text{BiSr}_2\text{CaCu}_2\text{O}_{8+\delta}$ (Bi2212) with $T_c \simeq 45$ K and $T_c \simeq 85$ K.¹¹ To explore whether this scenario also accounts for the Nernst signal N in terms of the relation $N \propto -m_d$, we consider the data for superconducting $\text{Nb}_{0.15}\text{Si}_{0.85}$ films taken above T_c .²³⁻²⁵ In Sec. II we sketch the theoretical background including the properties of the 0D-model. The neglect of thermal fluctuations implies that the model is applicable outside the critical regime only, that is sufficiently above T_c , the regime where the experimental data of $\text{La}_{1.91}\text{Sr}_{0.09}\text{CuO}_4$ and

Bi2212 was taken. Invoking quantum scaling the doping dependence of the minimum in the isothermal magnetization curves is also addressed. In Sec. III we present the analysis of the data based on the 0D-model, neglecting thermal fluctuations. The remarkable agreement with the measured isothermal magnetization curves, achieved for reasonable values of the model parameters, suggest that the occurrence of the minimum is attributable to a finite extent of the homogeneous domains. The doping dependence of the Bi2212 data is also consistent with the flow to a quantum phase transition in the underdoped limit. Furthermore it is shown that the profile of the isothermal Nernst signal of the superconducting $\text{Nb}_{0.15}\text{Si}_{0.85}$ film, treated as $N \propto -m_d$, is fully consistent with the 0D-model. Accordingly, singlet Cooper pairs subjected to orbital pair breaking in a 0D system are the main source of the observed diamagnetism and Nernst signal in an extended temperature window above T_c . Finally we show that the 0D-model provides for a variety of conventional and hole doped superconductors a universal perspective on the interplay between diamagnetism, Nernst signal, correlation length and the limited spatial extent of homogeneity. We close with a brief summary and some discussion.

II. THEORETICAL BACKGROUND

The fluctuation contribution to the free energy per unit volume of a homogeneous and anisotropic type II superconductor scales above T_c as^{2,3,5-7}

$$f = \frac{k_B T}{\xi_x \xi_y \xi_z} G\left(\frac{\xi_x \xi_y}{L_{H_z}^2}\right), \quad L_{H_z}^2 = \frac{\Phi_0}{H_z}, \quad (3)$$

where $G(z)$ is a scaling function of its argument and L_{H_z} is the magnetic field induced limiting length giving rise to a finite size effect.³¹ We assume that the magnetic field is applied along the z -axis. $\xi_{x,y,z}$ denote the correlation length along the respective axis in zero field. In the limit $\xi_x \xi_y \gg L_{H_z}^2 = \Phi_0/H_z$, attainable for sufficiently high fields, this expression reduces to

$$f \propto \frac{k_B T}{L_{H_z}^2 \xi_z} = \frac{k_B T H_z}{\Phi_0 \xi_z}, \quad (4)$$

because the zero field correlation lengths $\xi_x \xi_y$ cannot grow beyond $L_{H_z}^2$. In this limit the magnetization $m_d = -\partial f / \partial H_z$ tends to

$$\frac{m_d}{T} \propto -\frac{k_B}{\Phi_0 \xi_z}. \quad (5)$$

On the other hand, in the opposed limit $\xi_x \xi_y \ll L_{H_z}^2 = \Phi_0/H_z$ the scaling function adopts the limiting behavior, $G(z) \propto z^2$, to recover $m_d = -\chi_d H$. In this case we obtain

$$\frac{m_d}{T} \propto -\frac{2k_B \xi_x \xi_y}{\Phi_0 \xi_z} H_z. \quad (6)$$

Accordingly, in both the 3D and 2D case, where $\xi_z = d$ and d denotes the thickness of the superconducting sheets, the magnetization saturates at sufficiently high fields due to the magnetic field induced finite size effect, reducing the effective dimensionality D of the system from D to $D-2$.^{31,32} In this limit the system corresponds in $D = 3$ to independent superconducting cylinders of radius $L_{H_z} \propto (\Phi_0/H_z)^{1/2}$ and height ξ_z and in $D = 2$ with height $\xi_z = d$. Detailed calculations in $D = 2$ reveal that the crossover from the low to the high field limit occurs monotonically and according to that there is no minimum.⁴

So far we considered homogeneous systems only. In practice any real and highly anisotropic type II superconductor is homogenous within *e.g.* a cylinder of radius R and height d . Concentrating on temperatures sufficiently above T_c where thermal fluctuations in the phase and amplitude of the order parameter can be neglected, we are left with a 0D-system with an order parameter ψ which does not depend on the space variables. The temperature and magnetic field dependence follows then from the Ginzburg-Landau (GL) model for a 0D system as treated by Shmidt.^{9,33} The partition function in this case reads

$$Z = \int d\text{Re}(\psi) d\text{Im}(\psi) \text{Exp}(-f[\psi]), \quad (7)$$

with the GL free energy functional

$$f[\psi] = \frac{V}{k_B T} \left[r_0 \left(\ln \left(\frac{T}{T_c} \right) + \left(\frac{2\pi}{\Phi_0} \right)^2 \xi_0^2 \langle \mathbf{A}^2 \rangle \right) |\psi|^2 + \frac{u_0}{2} |\psi|^4 \right], \quad (8)$$

and

$$t = T/T_{c0} - 1, \quad \xi_0^2 = \frac{\hbar^2}{2mr_0}, \quad \xi^2 = \xi_0^2 t^{-1}. \quad (9)$$

\mathbf{A} is the vector potential and ξ the correlation length with amplitude ξ_0 . Setting

$$\begin{aligned} \psi^2 &= |z|^2 \frac{k_B T}{V}, \\ a &= r_0 \left(\ln \left(\frac{T}{T_c} \right) + \left(\frac{2\pi}{\Phi_0} \right)^2 \xi_0^2 \langle \mathbf{A}^2 \rangle \right), \\ u &= u_0 \left(\frac{k_B T}{V} \right), \end{aligned} \quad (10)$$

assuming $a > 0$ and $u > 0$ we obtain for the partition function the expression

$$Z = \frac{\pi^{3/2} k_B T}{V \sqrt{2u}} \text{Exp} \left(\frac{a^2}{2u} \right) \text{Erfc} \left(\frac{a}{\sqrt{2u}} \right). \quad (11)$$

$\text{Erfc}(z)$ is the complementary error function. The magnetization per unit volume follows then from the free energy

$F = -k_B T \ln(Z)$ in terms of

$$m_d = -\frac{1}{V} \frac{dF}{dH} = \frac{k_B T}{V} \cdot \frac{1}{Z} \frac{dZ}{dH}, \quad (12)$$

yielding

$$m_d = \frac{k_B T}{V} \left(\frac{a}{u} \frac{da}{dH} + \frac{d}{dH} \ln \left[\text{Erfc} \left(\frac{a}{\sqrt{2u}} \right) \right] \right). \quad (13)$$

Using the gauge $\mathbf{A} = (0, H_z x, 0)$ we obtain for a cylindrical homogenous domain with radius R , height d and a spherical domain with radius r

$$\langle \mathbf{A}^2 \rangle = \frac{H^2}{V} \int x^2 dV = a_4 H^2, \quad H = H_z, \quad (14)$$

where

$$a_4 = \begin{cases} R^2/4, & V = \pi R^2 d \\ r^2/5, & V = 4\pi r^3/3 \end{cases} \quad (15)$$

The magnetization expression (13) can then be rewritten as

$$m_d = a_3 \left(\frac{4a_1 H}{a_2^2} x + \frac{d}{dH} \ln [\text{Erfc}(x)] \right), \quad (16)$$

or

$$\begin{aligned} m_d &= \frac{2a_3 a_1}{a_2} \left(\frac{x}{a_1} - \ln \left(\frac{T}{T_c} \right) \right)^{1/2} \cdot \\ &\quad \left(2x + \frac{d}{dx} \ln [\text{Erfc}(x)] \right), \end{aligned} \quad (17)$$

where

$$\begin{aligned} x &= a_1 \left(\ln \left(\frac{T}{T_c} \right) + \left(\frac{H}{a_2} \right)^2 \right), \\ a_1 &= \frac{r_0 V^{1/2}}{\sqrt{2u_0 k_B T}}, \quad a_2 = \frac{\Phi_0}{2\pi \xi_0 a_4^{1/2}}, \quad a_3 = \frac{k_B T}{V}. \end{aligned} \quad (18)$$

In terms of the variable x , requiring the values of a_1 and a_2 , Eq. (16) adopts the simple scaling form

$$\frac{m_d}{H} = \frac{2a_3 a_1}{a_2^2} f(x), \quad f(x) = 2x + \frac{d}{dx} \ln [\text{Erfc}(x)], \quad (19)$$

with the limiting behavior

$$\begin{aligned} f(x)|_{x \rightarrow \infty} &= -1/x, \\ f(x)|_{x \rightarrow 0} &= -2/\sqrt{\pi} + (2 - 4/\pi)x. \end{aligned} \quad (20)$$

In the limit $x \rightarrow 0$ m_d reduces then to

$$m_d = -\frac{4a_3 a_1 H}{a_2^2 \sqrt{\pi}}, \quad (21)$$

consistent with $m_d = -\chi_d H$. Contrariwise, for $x = \infty$ it approaches

$$m_d = -\frac{2a_3 H}{a_2^2} \left(\ln \left(\frac{T}{T_c} \right) + \left(\frac{H}{a_2} \right)^2 \right)^{-1}. \quad (22)$$

Accordingly, the isothermal magnetization curves adopt for $T > T_c$ a minimum between the low and high field limits. This characteristic behavior also appears in Fig. 1. More specific the minimum at

$$x_m(t) = a_1 \left(\ln \left(\frac{T}{T_c} \right) + \left(\frac{H_m(t)}{a_2} \right)^2 \right) \quad (23)$$

follows from

$$\frac{dm_d}{dH} = 0, \quad (24)$$

yielding for sufficiently large a_1 the solution

$$x_m(T) = x_m(T_c) + 2a_1 \ln \left(\frac{T}{T_c} \right), \quad (25)$$

where

$$x_m(T_c) = a_1 \left(\frac{H_m(T_c)}{a_2} \right)^2 \simeq 1.02634. \quad (26)$$

Together with Eq. (23) and sufficiently large a_1 we obtain for the magnetic field $H_m(T)$, where the isothermal magnetization curves adopt a minimum, the relation

$$H_m(T) = a_2 \left(\frac{1.02634}{a_1} + \ln \left(\frac{T}{T_c} \right) \right)^{1/2}. \quad (27)$$

Accordingly, $H_m(T)$ does not vanish at T_c and the temperature dependent part is related with a_2 in Eq. (18) to the amplitude of the correlation length. This differs from the Gaussian approximation, valid for $u_0 = 0$ ($a_1 = \infty$). In this limit Eq. (22), rewritten in the form

$$m_d = -2a_3 \frac{H}{H_m^2(T)} \left(1 + \left(\frac{H}{H_m(T)} \right)^2 \right)^{-1}, \quad (28)$$

applies. Here $m_d(H, T)/T$ adopts at fixed temperature a minimum at

$$\begin{aligned} H_m(T) &= H_{m0} \ln^{1/2} \left(\frac{T}{T_c} \right), \\ H_{m0} &= a_2 = \frac{\Phi_0}{2\pi\xi_0 a_4^{1/2}}, \end{aligned} \quad (29)$$

between the low and high field behavior. Furthermore, in the cylindrical case is the ratio ξ_0^2/d according to Eqs. (15) and (29) given by

$$\frac{\xi_0^2}{d} = \frac{\Phi_0^2}{\pi k_B T} \frac{a_3}{a_2^2}. \quad (30)$$

The Gaussian expression Eq. (28) for the magnetization also implies that there is no particular depairing field. Indeed, the magnetization vanishes as $m_d = -2a_3/H$.

As aforementioned, the applicability of the Gaussian approximation requires that

$$\frac{r_0 V^{1/2}}{\sqrt{2u_0 k_B T}} \left(\ln \left(\frac{T}{T_c} \right) + \left(\frac{H}{a_2} \right)^2 \right) \rightarrow \infty \quad (31)$$

is very large. According to this, in systems with non-negligible quartic term u_0 it fails close to T_c in the low field limit. Considering highly anisotropic cuprates, such as $\text{La}_{2-x}\text{Sr}_x\text{CuO}_4$ with $x = 0.09$ and Bi2212 , this corresponds to the critical regime where a 3D-xy to 2D-xy crossover occurs and phase fluctuations dominate.³⁴ However, in this regime and for sufficiently large R even the full model fails because fluctuations are neglected. In the light of these considerations it is not unexpected that the Gaussian version of the model mimics the essential features of the field dependence of the magnetization shown in Fig. 1 well, namely the occurrence of the minimum between the low and high field behavior. The same qualitative agreement also emerges from the magnetization data of $\text{La}_{2-x}\text{Sr}_x\text{CuO}_4$ with $x = 0.06$,¹⁰ 0.055 ,¹⁰, Bi2212 with $T_c \approx 85$ K, underdoped Bi2212 with $T_c \approx 45$ K,¹¹ optimally and overdoped Bi2201La_y with $T_c \simeq 30$ K and $T_c \simeq 20$ K,¹¹ and Pb particles.¹³ To substantiate this qualitative agreement we explore in Sec. III the consistency of the measured isothermal magnetization curves of Pb,¹³ $\text{La}_{2-x}\text{Sr}_x\text{CuO}_4$ with $x = 0.09$ and Bi2212 ¹¹ with the outlined scenario for a zero dimensional system. Because the partition function (11) requires that $a > 0$ and with that according to Eqs. (10) and (15)

$$\ln \left(\frac{T}{T_c} \right) + \frac{\pi^2}{\Phi_0^2} \xi_0^2 R^2 H^2 > 0, \quad (32)$$

our analysis is essentially restricted to temperatures $T > T_c$.

One also expects that the diamagnetic contribution to the magnetization exhibits a characteristic doping dependence. Indeed, the phase transition line of $\text{La}_{2-x}\text{Sr}_x\text{CuO}_4$ is well described by the empirical relation

$$\begin{aligned} T_c(x) &= T_{\text{cm}} \left(1 - 2 \left(\frac{x}{x_m} - 1 \right)^2 \right) \\ &= \frac{2T_{\text{cm}}}{x_m^2} (x - x_u)(x_o - x), \end{aligned} \quad (33)$$

due to Presland *et al.*³⁵ At $T_c = 0$ the systems are expected to undergo a quantum phase transition. Here the amplitude of the correlation length ξ_0 diverges in a homogeneous system as⁶

$$\xi_0 \propto \delta^{-\bar{\nu}}, \quad (34)$$

while T_c scales according to

$$T_c \propto \delta^{\bar{\nu}}. \quad (35)$$

δ denotes the tuning parameter of the quantum phase transition with dynamic critical exponent z and correlation length exponent $\bar{\nu}$. Combining Eqs. (34) and (35), we obtain

$$\xi_0 \propto T_c^{-1/z}, \quad (36)$$

expected to apply in both, the underdoped ($x = x_u$) and overdoped ($x = x_o$) limits. Noting that ξ_0 enters $H_{m0} = a_2 = \Phi_0 / (\pi \xi_0 R)$ [Eqs. (15) and (29)], the magnetic field $H_m = H_{m0} (\ln(T/T_c))^{1/2}$, where the isothermal magnetization curves exhibit a minimum, the approach to the underdoped or overdoped limit should be observable. However, this behavior may be masked by means of the doping dependence of R , the radius of the homogeneous cylindrical domains.

III. DATA ANALYSIS

In this section we explore the consistency of isothermal magnetization and Nernst signal data with the predictions of the full 0D-model and its Gaussian version. We concentrate on the magnetization data of Pb nanoparticles,¹³ $\text{La}_{1.91}\text{Sr}_{0.09}\text{CuO}_4$,¹¹ and bulk $\text{BiSr}_2\text{CaCu}_2\text{O}_{8+\delta}$ (Bi2212) with $T_c \simeq 85$ K (slightly underdoped) and $T_c \simeq 45$ K (heavily underdoped),¹¹ and on Nernst signal data of a $\text{Nb}_{0.85}\text{Si}_{0.85}$ film.^{23–25}

A. Pb nanoparticles

The diamagnetism in Pb nanoparticles with average diameters ranging from 150 to 750 Å, sizes for which effects of finite-level spacing should be negligible, has been studied by Benardi *et al.*¹³ By means of high-field resolution superconducting quantum interference device (SQUID) measurements, isothermal magnetization curves were obtained for $T \gtrsim T_c$. Fig. 2 shows isothermal diamagnetic magnetization curves of the sample containing spherical nanoparticles with average radius $r = 375$ Å. For comparison we included fits to the Gaussian approximation Eq. (28) with the parameters listed in Table I and at $T = 7.11$ K to the 0D-model [Eq. (16)] yielding the parameters

$$\begin{aligned} a_1 &= 1303.7, \\ a_2 &= H_{m0} = 1407.46 \text{ Oe}, \\ a_3 &= 0.09 \text{ emu Oe/cm}^3, \\ a_5 &= 0.00015 \text{ emu/cm}^3, \end{aligned} \quad (37)$$

with $T_c = 7.09$ K in terms of the dotted line. To account for a temperature dependent background contribution we added to Eqs. (16) and (28) the parameter a_5 , which turns out to be rather small. The agreement of the 0D-model with the Gaussian approximation at $T = 7.11$ K also reveals that for $a_1 \approx 1300$ the limit $a_1 \rightarrow \infty$ is nearly attained. Indeed, the fit parameters a_2 , a_3 and a_5 as obtained from the 0D-model [Eq. (37)] and the Gaussian counterpart (see Table I) coincide nearly at $T = 7.11$ K.

On the other hand, considering H_m vs. T , from Eqs. (27) and (37) one expects that this agreement does not hold sufficiently close to T_c , because $H_m(T_c)$ does not vanish in the full 0D-model for any $a_1 > 0$ [Eq. (27)].

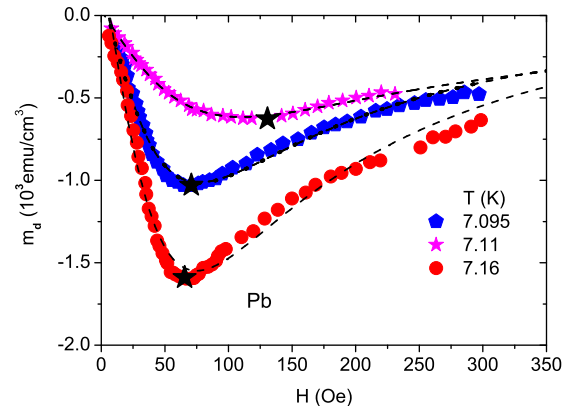


FIG. 2: (color online) Diamagnetic magnetization isotherms m_d vs. H for Pb nanoparticles with average radius $r = 375$ Å taken from Benardi *et al.*¹³ The dashed lines are fits to the Gaussian approximation Eq. (28) with the parameters listed in Table I. The dotted line at $T = 7.11$ K is a fit to Eq. (16) with the parameters listed in Table II with $T_c = 7.09$ K. The stars indicate the respective minima of the experimental data at H_m .

In Fig. 3 we observe that this behavior is well confirmed. Nevertheless we observe that the Gaussian approximation describes $H_m(T)$ rather well except very close to T_c . Contrariwise, in this regime thermal fluctuations are no longer negligible and even the 0D-model is not applicable. In this view it is gratifying that the Gaussian approximation describes $H_m(T)$ for sufficiently large a_1 and away from T_c rather well.

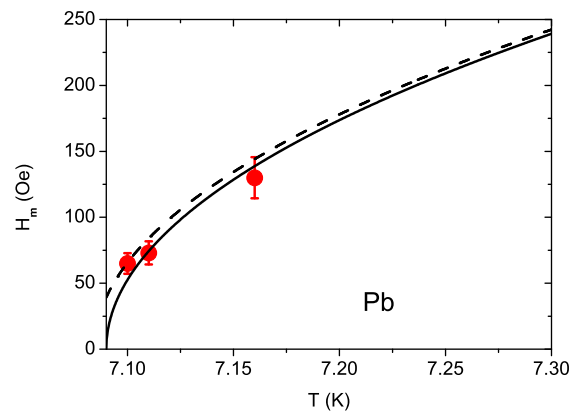


FIG. 3: (color online) H_m vs. T obtained from the magnetization data of the Pb nanoparticles. The dots mark the respective H_m 's of the experimental data shown in Fig. 2 with $\Delta H_m/H_m = 0.12$. The solid line is Eq. (29) with $a_2 = 1400$ Oe and $T_c = 7.09$ K, and the dashed one Eq. (27) with the parameters listed in Eq. (37).

Next we turn to the parameter $a_3 = k_B T/V$. In this context it should be recognized that in the resulting V

TABLE I: Fit parameters entering the Gaussian approximation [Eq. (28)] for Pb nanoparticles including the additive background correction a_5 . The amplitude $a_2 = H_{m0}$ is obtained from Eq. (29) with $T_c = 7.09$ K.

$T(K)$	$a_3(\text{emu Oe}/\text{cm}^3)$	$H_m(\text{Oe})$	$a_5(\text{emu}/\text{cm}^3)$	$a_2 = H_{m0}(\text{Oe})$
7.095	0.14	74.79	3.4×10^{-4}	2816.8
7.11	0.09	76.99	1.6×10^{-4}	1450.6
7.16	0.07	110.29	0.3×10^{-4}	1112.7

the packing density of the nanoparticles (spheres) is not taken into account. Indeed, the packing density η is the fraction of a volume filled by spheres. Noting that η varies from 0.055 for the loosest possible to 0.7405 for cubic close packing, it becomes clear that V is not simply related to the radius of the nanoparticles [$V = (4\pi/3)r^3$]. For $r = 375$ Å corresponding to 2.21×10^{-16} cm³ and $V = k_B T/a_3 \simeq 10.9 \times 10^{-15}$ cm³ ($a_3 = 0.09$ emuOe/cm³ and $T = 7.11$ K) we obtain $\eta \simeq 0.02$, revealing that in the sample considered here the packing density of the nanoparticles is worse than the loosest one. Given the uncertainty in the actual packing density we invoke for the amplitude of the correlation length the estimate $\xi_0 \simeq 1000$ Å,³⁶ yielding with Eqs. (15), (18) and $a_2 = H_{m0} = 1450$ Oe

$$r = \frac{\Phi_0 \sqrt{5}}{2\pi \xi_0 a_2} \simeq 508 \text{ Å}, \quad (38)$$

in comparison with $r = 375$ Å, estimated from AFM images of Pb nanoparticles onto a mica substrate.¹³

Even though the Hartree approximation works well for sufficiently high fields and away from T_c , it should be kept in mind that it fails inevitably in the zero field limit. Here the quartic term in the GL-functional is essential to remove the divergence of the correlation length ξ at T_c . Indeed, ξ cannot grow beyond r .

B. $\text{La}_{1.91}\text{Sr}_{0.09}\text{CuO}_4$

A glance at the isothermal magnetization curves shown in Figs. 1 and 2 uncover, surprisingly enough, the same characteristic behavior. Indeed, m_d decreases initially with increasing magnetic field, consistent with $m_d = -\chi_d H$, where χ_d is the diamagnetic susceptibility. However, as H increases m_d tends to a minimum at H_m and in excess of this characteristic field the magnetization increases and appears to approach zero. Noting that $1 \text{ A/m} = 10^{-3} \text{ emu/cm}^3$, the most striking difference concerns the magnitude of H_m which depends on the amplitude of the correlation length in terms of a_2 in Eq. (27). As ξ_0 in $\text{La}_{1.91}\text{Sr}_{0.09}\text{CuO}_4$ is around 25 Å,³⁷ compared to 1000 Å in Pb, the difference in H_m is not attributable to ξ_0 only but points to a substantial large value of $a_4^{1/2} = r/\sqrt{5}$ in Pb in comparison with $a_4^{1/2} = R/2$ [Eq. (15)] in $\text{La}_{2-x}\text{Sr}_x\text{CuO}_4$, where r is the radius of the nanoparticles, while R is the radius of the homogeneous cylindrical domains in the cuprate. To explore these

analogies and differences between the isothermal magnetization curves of Pb and $\text{La}_{2-x}\text{Sr}_x\text{CuO}_4$ with $x = 0.09$ quantitatively, we analyzed the data shown in Fig. 1 on the basis of the Gaussian model [Eq. (28)] yielding the parameters listed in Table II. For comparison we included in Fig. 4 a fit to the 0D-model [Eq. (16)] yielding at $T = 27$ K the parameters

$$\begin{aligned} a_1 &= 285.33, \\ a_2 &= 29.27 \text{ T}, \\ a_3 &= 455.67 \text{ AT/m}, \\ a_5 &= -17.30 \text{ A/m} \end{aligned} \quad (39)$$

where a_5 is the additive background correction. Though the parameter a_1 is considerably smaller than its Pb counterpart [Eq. (37)] we observe that the fit parameters a_2 , a_3 and a_5 as obtained from the 0D-model [Eq. (37)] and the Gaussian counterpart (see Table II) nearly coincide at $T = 27$ K. As the Gaussian approximation requires Eq. (31) to be fulfilled, this agreement is attributable to the fact that the temperatures considered here are considerably above $T_c \simeq 23$ K.

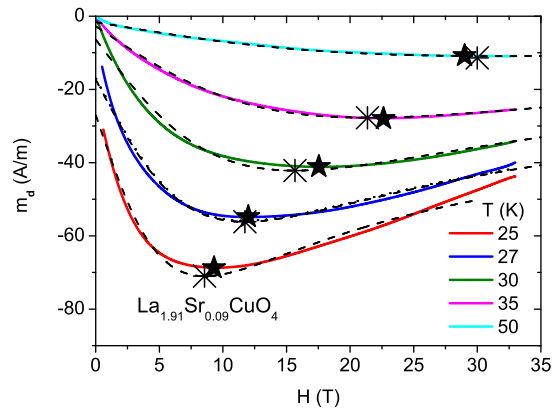


FIG. 4: (color online) Isothermal magnetization curves m_d vs. H at various temperatures above $T_c \simeq 23$ K of $\text{La}_{1.91}\text{Sr}_{0.09}\text{CuO}_4$ taken from Li *et al.*¹¹ ★ indicate the minima in the experimental and * of the Gaussian curves at the respective fixed temperatures. The dashed curves are fits to the Gaussian approximation [Eq. (28)] with the parameters listed in Table II and the dotted one to the 0D-model [Eq. (16)] with the parameters given in Eq. (39). In both models we included the additive background correction a_5 .

Given the estimate $a_2 = 31$ T we obtain with Eqs. (15)

TABLE II: Fit parameters entering Eq. (28) for $\text{La}_{1.91}\text{Sr}_{0.09}\text{CuO}_4$ including the additive background correction a_5 . The amplitude $a_2 = H_{m0}$ is obtained from Eq. (29) with $T_c = 23$ K.

T (K)	a_3 (AT/m)	$H_m(T)$ (T)	a_5 (A/m)	$a_2 = H_{m0}(T)$
25	376.66	8.56	-26.99	29.64
27	455.69	11.73	-17.29	29.29
30	561.41	15.67	-6.34	30.4
35	533.59	21.36	-2.73	32.96
50	294.95	30.01	-1.63	34.04

and (18)

$$R\xi_0 = \frac{\Phi_0}{\pi a_2} \simeq 2.13 \times 10^3 \text{ \AA}^2, \quad (40)$$

in comparison with $r\xi_0 \simeq 5.1 \times 10^5 \text{ \AA}^2$ in Pb corresponding to $a_2 = 940$ Oe. This difference is responsible for the large amplitude of a_2 of $H_m(T)$ [Eq. (27) in $\text{La}_{1.91}\text{Sr}_{0.09}\text{CuO}_4$. To estimate the radius R of the homogeneous domains we invoke for the amplitude of the in-plane correlation length the estimate $\xi_0 \approx 25 \text{ \AA}$ ³⁷ yielding with Eq. (40)

$$R = \frac{\Phi_0}{\pi \xi_0 a_2} \simeq 85 \text{ \AA}, \quad (41)$$

which is comparable to the amplitude of the in-plane correlation length. Noting that $1 \text{ A/m} = 10 \text{ erg}/(\text{cm}^3 \text{ T})$ we obtain for d the estimate

$$d = \frac{V}{\pi R^2} = 36 \text{ \AA}, \quad (42)$$

using $T = 27$ K and $a_3 = 455.69 \text{ AT/m}$, $V = \pi R^2 d = 8.2 \times 10^{-19} \text{ cm}^3$ and $R = 85 \text{ \AA}$. To check the reliability of these estimates, based on the amplitude $\xi_0 \approx 25 \text{ \AA}$ ³⁷ we invoke Eq. (30), yielding with $T = 27$ K, $\xi_0 = 25 \text{ \AA}$ and $d = 36 \text{ \AA}$ the estimate $a_3/a_2^2 = 0.49 \text{ A/mT}$, in reasonable agreement with $a_3/a_2^2 = 0.53 \text{ A/mT}$, resulting from the fit listed in Table II.

Given a_1 and a_2 , the temperature dependence of H_m , the magnetic field where the isothermal magnetization curves adopt a minimum, is readily calculated with Eq. (27) or Eq. (29). In Fig. 5, showing the resulting $H_m(t)$ we observe agreement with the experimental data. Noting that the magnitude of H_m is controlled by the amplitude $H_{m0} = \Phi_0/(\pi R\xi_0)$ and therewith by $R\xi_0$, the large difference between H_m of Pb and $\text{La}_{1.91}\text{Sr}_{0.09}\text{CuO}_4$ simply stems from the different $R\xi_0$ values, namely $r\xi_0 \simeq 5.1 \times 10^5 \text{ \AA}^2$ in Pb and $R\xi_0 \simeq 2.13 \times 10^3 \text{ \AA}^2$ in $\text{La}_{1.91}\text{Sr}_{0.09}\text{CuO}_4$. Except for this essential difference we observe a close analogy between the diamagnetic contribution to the isothermal magnetization in Pb nanoparticles and $\text{La}_{1.91}\text{Sr}_{0.09}\text{CuO}_4$. Clearly, this analogy breaks down close to T_c and in the zero field limit where thermal fluctuations dominate. Nevertheless, the observed analogy and the agreement with the 0D-scenario, requiring an order parameter ψ which does not depend on the space variables, reveals that in the temperature regime considered here fluctuations can be ignored.

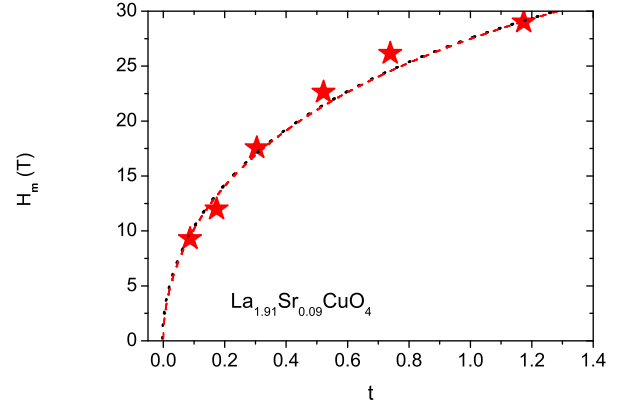


FIG. 5: (color online) H_m vs. $t = T_c/T - 1$ for $\text{La}_{1.91}\text{Sr}_{0.09}\text{CuO}_4$. The dotted line is Eq. (27) with $a_1 = 285.33$ and $a_2 = H_{m0} = 33$ T. The dashed line is the Gaussian approximation with $a_2 = 33$ T [Eq. (29)]. The stars denote the H_m values derived from the experimental data shown in Fig. 4.

C. Bi2212

To explore the established analogy between the diamagnetic contribution to the isothermal magnetization in Pb nanoparticles and $\text{La}_{2-x}\text{Sr}_x\text{CuO}_4$ with $x = 0.09$ further we extend the analysis to the Bi2212 data of Li *et al.*¹¹ shown in Fig. 6. We include fits of the Gaussian model [Eq. (28)] yielding the parameters listed in Table III and a fit to the 0D-model [Eq. (16)] yielding at $T = 95$ K,

$$\begin{aligned} a_1 &= 311.06, \\ a_2 &= 44.32 \text{ T}, \\ a_3 &= 945.29 \text{ AT/m}, \\ a_5 &= -6.80 \text{ A/m}. \end{aligned} \quad (43)$$

a_5 is again an additive background correction. Though the parameter a_1 is considerably smaller than its Pb counterpart [Eq. (37)] we observe that the fit parameters a_2 , a_3 and a_5 as obtained from the 0D-model [Eq. (43)] and the Gaussian counterpart (Table III) nearly coincide at $T = 95$ K. In analogy to $\text{La}_{2-x}\text{Sr}_x\text{CuO}_4$ we attribute this agreement to the fact that the temperatures considered here are considerably above $T_c \simeq 85$ K. Indeed, the

magnetic penetration depth measurements of Osborn *et al.*³⁸ and their analysis,²¹ clearly reveal that the temperature window around T_c , where thermal fluctuations dominate, is roughly 1 K only.

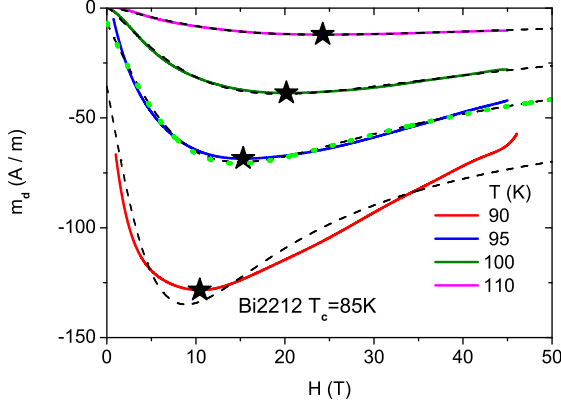


FIG. 6: (color online) The solid lines show m_d vs. H at various temperatures above $T_c \simeq 85$ K of Bi2212 taken from Li *et al.*¹¹. \star indicates the minimum in the isotherms at the respective fixed temperatures. The dashed curves are fits to the Gaussian approximation [Eq. (28)] with the parameters listed in Table III and the dotted one to the 0D-model [Eq. (16)] with the parameters given in Eq. (43). In both models we included the additive background correction a_5 .

Using $a_2 = 45$ T we obtain with Eqs. (15) and (18)

$$R\xi_0 = \frac{\Phi_0}{\pi a_2} \simeq 1.46 \times 10^3 \text{ \AA}^2, \quad (44)$$

in comparison with $r\xi_0 \simeq 3.7 \times 10^5 \text{ \AA}^2$ for Pb corresponding to $a_2 = 940$ Oe, and $R\xi_0 \simeq 2.13 \times 10^3 \text{ \AA}^2$ for $\text{La}_{2-x}\text{Sr}_x\text{CuO}_4$ with $T_c \simeq 23$ K [Eq. (40)]. To estimate the radius R of the homogeneous domains we invoke $R/\xi_0 \simeq 15$,²⁰ entering the rounding of the specific heat singularity, to obtain

$$R \simeq 148 \text{ \AA} \quad (45)$$

and $\xi_0 \simeq 10 \text{ \AA}$, in comparison with $\xi_0 \simeq 7 \text{ \AA}$,²¹ derived from the magnetic penetration depth. Noting that $1 \text{ A/m} = 10 \text{ erg}/(\text{cm}^3\text{T})$ we obtain for $T = 95$ K and $a_3 = 945 \text{ AT/m}$, $V = 1.38 \times 10^{-18} \text{ cm}^3$ and with $R = 148 \text{ \AA}$ for d the estimate

$$d = \frac{V}{\pi R^2} = 19 \text{ \AA}. \quad (46)$$

To check the reliability of these estimates, based on $R/\xi_0 \simeq 15$,²⁰ we invoke Eq. (30), yielding with $T = 95$ K, $\xi_0 = R/15 \text{ \AA} = 9.9 \text{ \AA}$ and $d = 19 \text{ \AA}$, $a_3/a_2^2 = 0.49 \text{ A/mT}$, in reasonable agreement with $a_3/a_2^2 = 0.47 \text{ A/mT}$, resulting from Table IV.

Given the estimates for a_1 and a_2 the temperature dependence of H_m , the magnetic field where the isothermal

magnetization curves adopt a minimum, is readily calculated with Eq. (27) or Eq. (29). In Fig. 7, showing the resulting $H_m(t)$ we observe excellent agreement with the values derived from the experimental data.

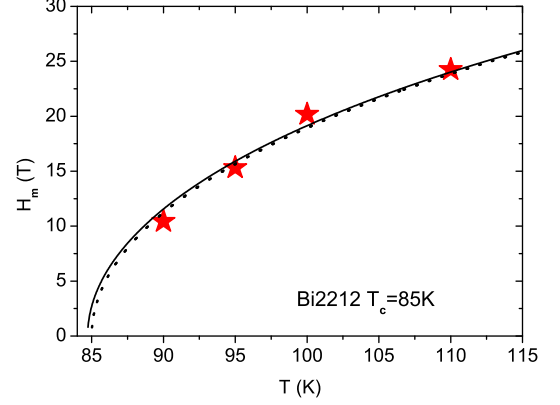


FIG. 7: (color online) H_m vs. t for Bi2212 with $T_c \simeq 85$ K. The solid line is Eq. (27) with $a_1 = 311.06$ and $a_2 = 45$ T. The stars denote the H_m values derived from the experimental data as shown in Fig. 4. The dotted curve is the Gaussian approximation [Eq. (29)].

To explore the effects of doping we consider the isothermal magnetization data of Li *et al.*¹¹ for Bi2212 with $T_c = 45$ K shown in Fig. 8. We include fits of the Gaussian model [Eq. (28)] yielding the parameters listed in Table IV and a fit to the 0D-model [Eq. (16)] yielding at $T = 52.5$ K,

$$\begin{aligned} a_1 &= 100.55, \\ a_2 &= 21.93 \text{ T}, \\ a_3 &= 395.01 \text{ AT/m}, \\ a_5 &= -53.76 \text{ A/m}. \end{aligned} \quad (47)$$

a_5 is again an additive background correction. Though the parameter a_1 is considerably smaller than in Bi2212 with $T_c = 85$ K [Eq. (43)] we observe that the fit parameters a_2 , a_3 and a_5 as obtained from the 0D-model [Eq. (37)] and the Gaussian counterpart (Table IV) are close at $T = 52.5$ K.

For this reason the temperature dependence of H_m depicted in Fig. 9 is reasonably well described by the Gaussian approximation Eq. (29) with $a_2 = 25$ T, yielding the estimate

$$R\xi_0 = \frac{\Phi_0}{\pi a_2} \simeq 2.6 \times 10^3 \text{ \AA}^2, \quad (48)$$

in comparison with $R\xi_0 \simeq 1.46 \times 10^3 \text{ \AA}^2$ for Bi2212 with $T_c \simeq 85$ K.

Noting that Bi2212 with $T_c = 85$ K is close to optimum doping while the sample with $T_c = 45$ K is underdoped, the amplitude H_{m0} is expected to exhibit the flow to the quantum phase transition at $T_c = 0$. Supposing that the

TABLE III: Fit parameters entering Eq. (28) for slightly underdoped Bi2212 including the additive background correction a_5 . The amplitude $a_2 = H_{m0}$ is obtained from Eq. (29) with $T_c = 85$ K.

T (K)	a_3 (A/mT)	H_m (T)	a_5 (A/m)	$a_2 = H_{m0}$ (T)
90	882.09	8.89	-35.7	37.18
95	945.60	14.93	-6.79	44.77
100	788.35	19.64	+1.11	48.72
110	322.64	24.5	+1.07	48.25

TABLE IV: Fit parameters entering the Gaussian approximation [Eq. (28)] for heavily underdoped Bi2212 including the additive background correction a_5 . The amplitude $a_2 = H_{m0}$ is obtained from Eq. (29) with $T_c = 45$ K.

T (K)	a_3 (A/mT)	H_m (T)	a_5 (A/m)	$a_2 = H_{m0}$ (T)
47.5	315.68	4.66	-84.35	20.04
50	362.76	6.61	-67.7	20.36
52.5	392.59	8.65	-54.11	22.03
55	467.32	11.07	-40.5	24.17
60	548.43	16.19	-18.89	30.18

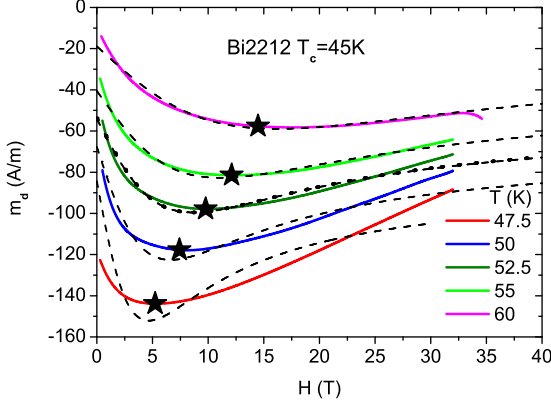


FIG. 8: (color online) The solid lines show the isothermal magnetization curves of underdoped Bi2212 with $T_c \simeq 45$ K taken from Li *et al.*¹¹. ★ indicates the minimum in the isotherms at the respective temperatures. The dashed curves are fits to the Gaussian approximation [Eq. (28)] with the parameters listed in Table IV and the dotted one to the 0D-model [Eq. (16)] with the parameters given in Eq. (47). In both models we included the additive background correction a_5 .

doping dependence of R , the radius of the homogeneous cylindrical domains is weak $a_2 = H_{m0}$ scales according to Eqs. (15), (29) and (36) as

$$a_2 = H_{m0} \propto T_c^{1/z}, \quad (49)$$

and $a_3/(a_2^2 T)$ scales according to Eqs. (30) and (36) as

$$a_3/(a_2^2 T) \propto T_c^{-2/z}. \quad (50)$$

In Fig. 10 we plotted our estimates for $a_2 = H_{m0}$ and $a_3/(a_2^2 T)$ vs. T_c revealing consistency with the expected flow to the quantum critical point with $z = 1$ over an unexpectedly large T_c range.

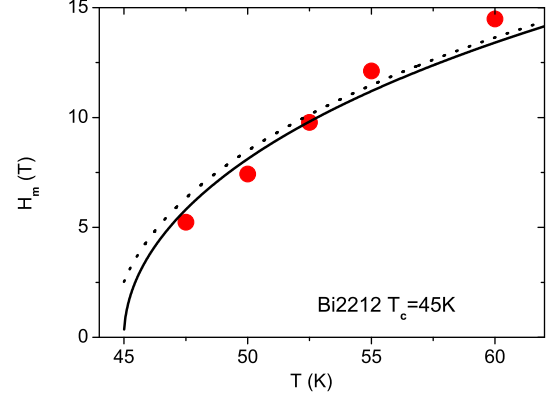


FIG. 9: (color online) H_m vs. T for Bi2212 with $T_c \simeq 45$ K derived from the isothermal magnetization data Li *et al.*¹¹. The dotted line is Eq. (27) with $a_1 = 100.55$ and $a_2 = 25$ T. The solid line is the Gaussian approximation [Eq. (27)].

D. $\text{Nb}_{0.15}\text{Si}_{0.85}$

The observation of a finite Nernst signal in the normal state of cuprates has revived interest in the study of superconducting fluctuations.^{29,30} In conventional superconductors the survival of Cooper pairs above T_c has been predominantly examined through the phenomena of paraconductivity³⁹ and diamagnetism.¹³ To explore the relationship between the Nernst signal and magnetization we consider the data of Pourret *et al.*^{23–25} for a 350 Å thick $\text{Nb}_{0.15}\text{Si}_{0.85}$ film with $T_c \simeq 0.38$ K. In this amorphous superconductor the usual Nernst signal due to normal quasiparticles is negligible.^{23–25} Furthermore, due to the small Hall angle is the Nernst signal simply related to the Peltier coefficient α_{xy} in terms of

$$N = \nu H = \frac{\alpha_{xy}}{\sigma_{xx}}. \quad (51)$$

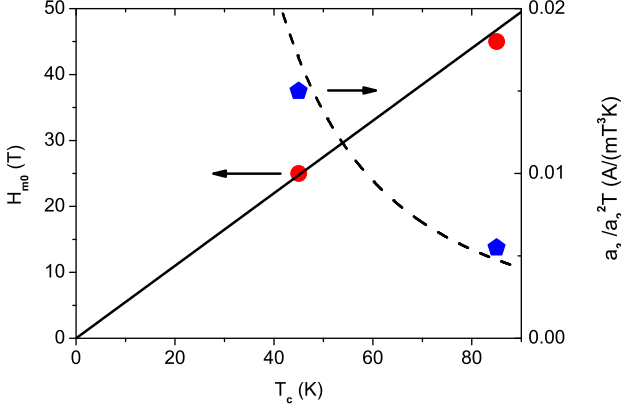


FIG. 10: (color online) $a_2 = H_{m0}$ vs. T_c and $a_3/(a_2^2 T)$ for underdoped and nearly optimally doped Bi2212. The solid line is $H_{m0} = a_2 = 0.55T_c$ and the dashed one $a_3/(a_2^2 T) = 34.43/T_c^2$. a_2 and a_3 are taken from Table III at $T = 95$ K and Table IV at $T = 52.5$ K.

ν denotes the Nernst coefficient and σ_{xx} the conductivity. Above T_c , as the conductivity changes only weakly with temperature and magnetic field, the evolution of the Peltier coefficient is mainly controlled by the Nernst coefficient.^{23–25} In Fig. 11 we show the isothermal Nernst signal curves for temperatures above T_c . For comparison we included fits to the Gaussian approximation for the magnetization [Eq. (28)] with the parameters listed in Table V and at $T = 0.43$ K to the 0D-model [Eq. (16)] in terms of the dotted line, yielding the parameters

$$\begin{aligned} a_1 &= 355.67, \\ a_2 &= H_{m0} = 1.085 \text{ T}, \\ a_3 &= -0.042 \mu\text{VT/K}, \\ a_5 &= 0.003 \mu\text{V/K}. \end{aligned} \quad (52)$$

With the exception of $T = 0.41$ K, which is rather close to $T_c \simeq 0.38$ K where fluctuations are expected to contribute, we observe remarkable agreement and a justification of the Gaussian approximation. This agreement also reveals that sufficiently above T_c the Nernst signal is proportional to the negative magnetization. Indeed, Fig. 11 clearly reveals that the Nernst signal mirrors the profile of the isothermal magnetization and exhibits the characteristic maximum at H_m . Because the Gaussian approximation is applicable, the temperature dependence of H_m should follow from Eq. (29).

In Fig. 12 we plotted H_m vs. T and included a fit to Eq. (29) yielding $H_{m0} = 1.28$ T, in reasonable agreement with the estimates listed in Table V. It then follows that

$$R\xi_0 = \frac{\Phi_0}{\pi H_{m0}} \simeq 5.2 \times 10^4 \text{ \AA}^2, \quad (53)$$

in comparison with $r\xi_0 \simeq 3.7 \times 10^5 \text{ \AA}^2$ for Pb corresponding to $a_2 = 940$ Oe, $R\xi_0 \simeq 2.13 \times 10^3 \text{ \AA}^2$ for $\text{La}_{2-x}\text{Sr}_x\text{CuO}_4$ with $T_c \simeq 23$ K [Eq. (40)], $R\xi_0 \simeq 1.46 \times$

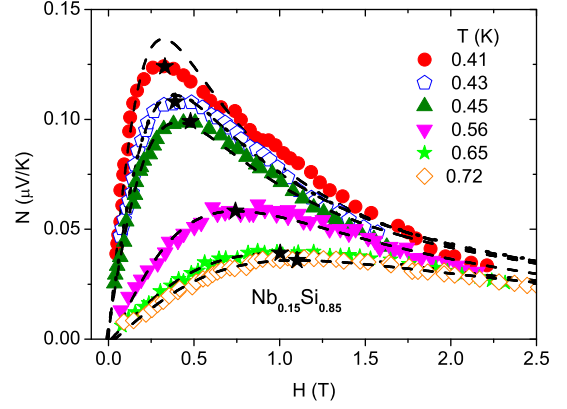


FIG. 11: (color online) Isothermal Nernst signal curves of a 350 Å thick $\text{Nb}_{0.15}\text{Si}_{0.85}$ film with $T_c \simeq 0.38$ K taken from Pourret *et al.*^{23–25} The solid lines are fits to the Gaussian approximation [Eq. (28)] with the parameters listed in Table V. ★ indicates the maximum in the measured isotherms at the respective temperatures.

10^3 \AA^2 in Bi2212 with $T_c = 85$ K, and $R\xi_0 \simeq 2.6 \times 10^3 \text{ \AA}^2$ with $T_c = 45$ K. To estimate the radius R of the homogeneous domains we invoke $\xi_0 \simeq 130 \text{ \AA}$,^{23–25} to obtain

$$R \simeq 400 \text{ \AA}, \quad (54)$$

in comparison with a limiting lateral length of 900 Å, obtained from a detailed finite size scaling analysis of the magnetic field dependence of the conductivity in a 125 Å thick $\text{Nb}_{0.15}\text{Si}_{0.85}$ film.²² This limiting length also implies that the evidence for a magnetic field driven quantum phase transition in this system is constricted by the resulting finite size effect.⁴⁰

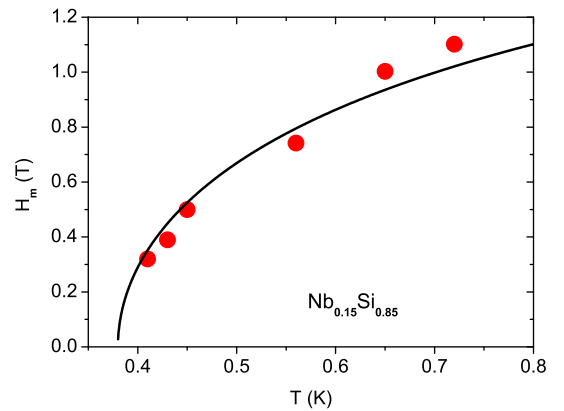


FIG. 12: (color online) H_m vs. T for the $\text{Nb}_{0.15}\text{Si}_{0.85}$ film with $T_c \simeq 0.38$ K derived from the data shown in Fig. 11. The solid line is Eq. (27) with $H_{m0} = 1.28$ T.

Remarkably, the Gaussian version of the 0D-model describes the profile of the isothermal Nernst signal above

TABLE V: Fit parameters a_3 , H_m , and a_5 entering the Gaussian approximation [Eq. (28)] for the $\text{Nb}_{0.15}\text{Si}_{0.85}$ film. a_5 is the additive background correction. H_{m0} follows from Eq. (29).

T (K)	a_3 ($\mu\text{VT/K}$)	H_m (T)	a_5 ($\mu\text{V/K}$)	$a_2 = H_{m0}$ (T)
0.41	-0.044	0.320	0	1.161
0.43	-0.042	0.386	0.003	1.098
0.45	-0.038	0.403	0.006	0.980
0.56	-0.047	0.742	0.003	1.192
0.65	-0.041	1.003	-0.001	1.369
0.72	-0.043	1.102	-0.003	1.378

T_c and the temperature dependence of H_m in terms of $N \propto -m_d$ very well. In the low field limit this relationship transforms with Eq. (28) to

$$N \propto -m_d \propto -\frac{2a_3\pi^2\xi^2R^2}{\Phi_0^2}H, \quad (55)$$

which differs from the Gaussian fluctuation contribution $N \propto H\xi^2$, valid close to T_c and in the zero magnetic field limit.^{27,28}

To substantiate the neglect of thermal fluctuations in the 0D-model further we invoke the Ginzburg criterion for a 2D-system, $|\Delta T|/T_c \simeq |2G_i \ln(G_i)|$. ΔT is the range of temperatures where thermal fluctuations are essential and $G_i = (e^2/23\hbar)R_n$ is the Ginzburg-Levanyuk parameter for a dirty film with normal state resistance R_n .⁹ With $R_n = 0.3 \text{ k}\Omega$ ^{24,25} and $T_c = 0.38 \text{ K}$ we obtain $|\Delta T| \approx 0.01 \text{ K}$. As a result the Nernst signal curves shown in Fig. 11 were taken outside the critical regime where fluctuations dominate.

IV. SUMMARY AND DISCUSSION

Noting that in cuprate and amorphous conventional superconductors the spatial extent of the homogeneous domains is limited,^{8,16–22} we explored the applicability of the 0D-model, neglecting thermal fluctuations, to describe the isothermal magnetization and Nernst signal curves above T_c . Sufficiently above T_c we observed that for both models, the full 0D-model and its Gaussian version, describe the essential features of the curves, including the temperature dependence of the minimum in the magnetization and maximum in the Nernst signal curves at H_m , rather well. The essential difference between the magnetization curves of the Pb nanoparticles and the bulk cuprates was traced back to the product between the amplitude ξ_0 of the correlation length and the radius R of the spatial restriction. Indeed, the magnitude of $H_m \simeq H_{m0} \ln^{1/2}(T/T_c)$ is controlled by the amplitude H_{m0} . It adopts in the Pb nanoparticles the value $H_{m0} \propto 1/\xi_0 r \approx 10^{-6} \text{ \AA}^{-2}$ compared to $1/\xi_0 R \approx 10^{-5}$ in the 350 \AA thick $\text{Nb}_{0.15}\text{Si}_{0.85}$ film, and $1/\xi_0 R \approx 10^{-3} \text{ \AA}^{-2}$ in the cuprates considered here. Indeed, as shown in Fig. 13, the data for H_m vs. T , depicted in Figs. 3, 5, 7, 9, and 12 for Pb nanoparticles, $\text{La}_{1.91}\text{Sr}_{0.09}\text{CuO}_4$, Bi2212 and $\text{Nb}_{0.15}\text{Si}_{0.85}$, tend to fall on a single curve,

plotted as H_m/H_{m0} vs. $t = T/T_c - 1$. This curve is even well described by the Gaussian version of the 0D-model [Eq. (29)]. Thus, for a variety of conventional and hole doped cuprate superconductors it gives a universal perspective on the interplay between diamagnetism, Nernst signal, correlation length, and the limited spatial extent of homogeneity.

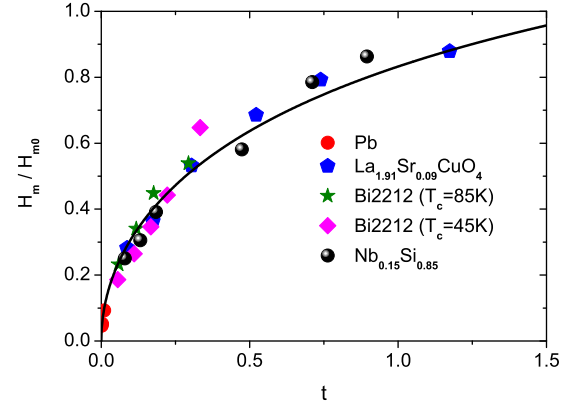


FIG. 13: (color online) H_m/H_{m0} vs. $t = T/T_c - 1$ for the data shown in Figs. 3, 5, 7, 9, and 12. The solid curve is $H_m/H_{m0} = \ln^{1/2}(1+t)$ corresponding to the Gaussian approximation [Eq. (29)].

Although the assumption of an order parameter which does not depend on the spatial variables fails in the fluctuation dominated temperature window close to T_c , we established overall agreement between the 0D-model, the isothermal magnetization and the Nernst signal treated as $N \propto -m_d$. As a consequence, thermal fluctuations associated with the amplitude and the phase of the order parameter do not contribute significantly in the temperature and magnetic field regimes considered here. The agreement also implies that singlet Cooper pairs in a 0D system subjected to orbital pair breaking are the main source of the observed diamagnetism and Nernst signal in an extended temperature window above T_c . The monotonic decrease of the magnetization m_d and the Nernst signal N with magnetic field H also reveals that there is no particular depairing field. Indeed, N and m_d vanish as $|m_d| \propto |N| \propto 2a_3/H$ [Eq. (28)]. Noting that $N \propto -m_d$ also holds for Gaussian fluctuations close to T_c and in the

zero magnetic field limit,²⁸ we have shown that it applies even outside the fluctuation dominated regime.

Clearly, the outlined approach cannot distinguish between intrinsic and extrinsic inhomogeneities, or whether the detected restricted extent of the homogeneous regions reflect an intimate relationship to superconductivity. However, it implies that the reduced dimensionality is not only responsible for the smeared zero field transitions seen in the specific heat,^{19,20} in the temperature dependence of the magnetic penetration depths,^{19,21} and the resistive transition,²² but also accounts for the ob-

served characteristic minimum in the isothermal magnetization curves and the corresponding maximum in the Nernst signal.

V. ACKNOWLEDGEMENTS

The authors acknowledge stimulating and helpful discussions with H. Keller. This work was partly supported by the Swiss National Science Foundation.

-
- * Electronic address: toni.schneider@swissonline.ch
- ¹ M. Tinkham, *Introduction to Superconductivity* (McGraw-Hill, New York, 1996), Chap. 8.
 - ² D. S. Fisher, M. P. A. Fisher, and D. A. Huse, Phys. Rev. B **43**, 130 (1991).
 - ³ T. Schneider and H. Keller, Inter. J. Mod. Phys. B **8**, 487 (1994).
 - ⁴ A. E. Koshelev, Phys. Rev. B **50**, 506 (1994).
 - ⁵ J. Hofer, T. Schneider, J. M. Singer, M. Willemin, H. Keller, T. Sasagawa, K. Kishio, K. Conder, and J. Karpinski, Phys. Rev. B **62**, 631 (2000).
 - ⁶ T. Schneider and J. M. Singer, *Phase Transition Approach To High Temperature Superconductivity*, (Imperial College Press, London, 2000).
 - ⁷ T. Schneider, in: *The Physics of Superconductors*, edited by K. Bennemann and J. B. Ketterson (Springer, Berlin, 2004).
 - ⁸ T. Schneider and J. M. Singer, Physica C **341**, 87 (2000).
 - ⁹ A. Larkin and A. Varlamov, *Theory of Fluctuations in Superconductors*, Clarendon, Oxford, 2005.
 - ¹⁰ L. Li, J. G. Checkelsky, S. Komiya, Y. Ando, and N. P. Ong, Nature Physics, **3**, 311 (2007).
 - ¹¹ L. Li, Y. Wang, S. Komiya, S. Ono, Y. Ando, G. D. Gu, and N. P. Ong, Phys. Rev. B **81**, 054510 (2010).
 - ¹² A. Lascialfari, A. Rigamonti, L. Romanò, P. Tedesco, A. Varlamov, and D. Embriaco, Phys. Rev. B **65**, 144523 (2002).
 - ¹³ E. Bernardi, A. Lascialfari, A. Rigamonti, L. Romanò, V. Iannotti, G. Ausanio, and C. Luponio, Phys. Rev. B **74**, 134509 (2006).
 - ¹⁴ A. Lascialfari, T. Mishonov, A. Rigamonti, P. Tedesco, and A. Varlamov, Phys. Rev. B **65**, 180501(R) (2002).
 - ¹⁵ E. Bernardi, A. Lascialfari, A. Rigamonti, L. Romanò, M. Scavini, and C. Oliva, Phys. Rev. B **81**, 064502 (2010).
 - ¹⁶ S. H. Pan, J. P. O'Neal, R. L. Badzey, C. Chamon, H. Ding, J. R. Engelbrecht, Z. Wang, H. Eisaki, S. Uchida, A. K. Gupta, K. W. Ng, E. W. Hudson, K. M. Lang, and J. C. Davis, Nature (London) **413**, 282 (2001).
 - ¹⁷ K. M. Lang, V. Madhavan, J. E. Hoffman, E. W. Hudson, H. Eisaki, S. Uchida, and J. C. Davis, Nature (London) **415**, 412 (2002).
 - ¹⁸ I. Iguchi, A. Sugimoto, and H. Sato, J. Low Temp. Phys. **131** 451 (2003).
 - ¹⁹ T. Schneider, J. Supercond. **17**, 41 (2004).
 - ²⁰ J. W. Loram, J. L. Tallon, and W. Y. Liang, Phys. Rev. B **69**, 060502(R) (2004).
 - ²¹ T. Schneider and D. Di Castro, Phys. Rev. B **69**, 024502 (2004).
 - ²² T. Schneider, Phys. Rev. B **80**, 214507 (2009).
 - ²³ A. Pourret, H. Aubin, J. Lesueur, C. A. Marrache-Kikuchi, L. Bergé, L. Dumoulin, and K. Behnia, Nature Physics **2**, 683 (2006).
 - ²⁴ A. Pourret, H. Aubin, J. Lesueur, C. A. Marrache-Kikuchi, L. Bergé, L. Dumoulin, and K. Behnia, Phys. Rev. B, **76**, 214504 (2007).
 - ²⁵ A. Pourret, P. Spathis, H. Aubin, and K. Behnia, New J. Phys. **11**, 055071 (2009).
 - ²⁶ C. Caroli and K. Maki, Phys. Rev. **164**, 591 (1967).
 - ²⁷ S. Ullah and A. T. Dorsey, Phys. Rev. Lett. **65**, 2066 (1990); Phys. Rev. B **44** 262 (1991).
 - ²⁸ I. Ussishkin, S. L. Sondhi, and D. A. Huse, Phys. Rev. Lett. **89**, 287001 (2002).
 - ²⁹ Y. Wang, L. Li, M. J. Naughton, G. D. Gu, S. Uchida, and N. P. Ong, Phys. Rev. Lett. **95**, 247002 (2005).
 - ³⁰ Y. Wang, L. Li, and N. P. Ong, Phys. Rev. B **73**, 024510 (2006).
 - ³¹ T. Schneider, J. Phys.: Condens. Matter **20**, 423201 (2008).
 - ³² P. A. Lee and S. R. Shenoy, Phys. Rev. Lett. **28**, 1025 (1972).
 - ³³ V. V. Shmidt, in *Proceedings of the IXX International Conference on Low Temperature Physics*, edited by M. P. Malkov, L. P. Pitaevski, and A. Shalnikov (Viniti Publishing House, Moscow, 1967), Vol. II B, p. 205.
 - ³⁴ S. Weyeneth, T. Schneider, and E. Giannini, Phys. Rev. B **79**, 214504 (2009).
 - ³⁵ M. R. Presland, J. L. Tallon, R. G. Buckley, R. S. Liu, and N. E. Flower, Physica C **176**, 95 (1991).
 - ³⁶ H. R. Kerchner and D. M. Ginsberg, Phys. Rev. B **8**, 3190 (1973).
 - ³⁷ S. Kohout, T. Schneider, J. Roos, H. Keller, T. Sasagawa, and H. Takagi, Phys. Rev. B **76**, 064513 (2007).
 - ³⁸ K. D. Osborn, D. J. Van Harlingen, V. Aji, N. Goldenfeld, S. Oh, and J. N. Eckstein, Phys. Rev. B **68**, 144516 (2003).
 - ³⁹ R. E. Glover, Phys. Lett. **25A**, 542 (1967).
 - ⁴⁰ H. Aubin, C. A. Marrache-Kikuchi, A. Pourret, K. Behnia, L. Bergé, L. Dumoulin, and J. Lesueur, Phys. Rev. B **73**, 094521 (2006).